Cumulants of conserved charges in hydrodynamic simulations

Renan Hirayama [,1] Frédérique Grassi [,2] Willian Matioli Serenone,[2] and Jean-Yves Ollitrault [3]

[1]*Helmholtz Forschungsakademie Hessen für FAIR (HFHF), Frankfurt Institute for Advanced Studies, Ruth-Moufang-Strasse 1, 60438 Frankfurt am Main, Germany*

[2]*Instituto de Fìsica, Universidade de São Paulo, Rua do Matão 1371, 05508-090 São Paulo, Brazil*

[3]*Université Paris Saclay, CNRS, CEA, Institut de physique théorique, 91191 Gif-sur-Yvette, France*

We introduce a fast and simple method of computing cumulants of net-proton or net-charge fluctuations in event-by-event hydrodynamic simulations of heavy-ion collisions. One evaluates the mean numbers of particles in every hydrodynamic event. Cumulants are then expressed as a function of these mean numbers. We implement the corrections due to global conservation laws. The method is tested using ideal hydrodynamic simulations of Au+Au collisions at $\sqrt{s_{NN}} = 200A$ GeV with the NeXSPheRIO code. Results are in good agreement with experimental data on net-proton and net-charge fluctuations by the STAR Collaboration.

I. INTRODUCTION

One of the primary goals of relativistic heavy-ion collisions is to study experimentally the thermodynamic properties of the theory of strong interactions, quantum chromodynamics (QCD). In particular, one hopes to relate the event-to-event fluctuations of a physical quantity, for example the net electric charge observed in a specific detector [1], to the thermodynamic fluctuations of that quantity at some temperature. The interest in thermodynamic fluctuations is twofold. First, they diverge in the vicinity of a phase transition [2] and might help locate a critical point in the QCD phase diagram [3]. This is one of the main goals of the beam energy scan at the Relativistic Heavy Ion Collider (RHIC) [4], where hints of enhanced fluctuations have been reported [5,6]. Second, at zero baryon chemical potential, thermodynamic fluctuations can be calculated from first principles in lattice QCD [7,8], and these calculations have been compared with experimental measurements [9–12].

Hydrodynamic models [13,14] have been notoriously successful in reproducing bulk observables of relativistic heavy-ion collisions [15–17]. Therefore, hydrodynamics seems a natural framework for modeling the fluctuations which are measured experimentally: One describes the strongly coupled quark-gluon matter formed in the collision as a relativistic fluid, which expands freely and cools down until it reaches the so-called freeze-out temperature, where it is converted into hadrons. Typical fluctuation observables depend on the temperature, not on the fluid velocity, because they involve particle numbers, not momenta [18]. This implies that in a hydrodynamic calculation, fluctuations are essentially those of a hadron gas at the freeze-out temperature [19]. Now, first-principles calculations of thermodynamic fluctuations in QCD give results in agreement with a hadron gas [20] in the relevant temperature range. This suggests that hydrodynamics is a valid framework for investigating fluctuations.

A full hydrodynamic calculation has significant advantages over a simple thermodynamic calculation: First, the modification of the momentum distribution due to the collective fluid velocity is taken into account, so that the kinematic cuts inherent to particle detectors can be properly implemented [21]. Second, effects of event-to-event fluctuations, which are not taken into account in lattice calculations [10], can be modeled realistically [22,23]. However, hydrodynamics is a continuous description, while fluctuation observables involve discrete particle numbers [18]. Therefore, evaluating these observables within a hydrodynamic model is not straightforward. The goal of this article is to introduce a simple and efficient method to evaluate cumulants in event-by-event hydrodynamics. We illustrate its interest by comparing theoretical calculations with experimental results for net-proton [24] and net-charge [1] fluctuations in Au+Au collisions at $\sqrt{s_{NN}} = 200A$ GeV.

The fully consistent way of studying fluctuations with hydrodynamics would be to include them in the hydrodynamic description itself [25–29]. Hydrodynamic fluctuations are large near a critical point [30–32], and have non-trivial effects even in the absence of a critical point [33–36]. Here, we postulate that fluctuations in heavy-ion collisions originate mostly from the initial state, and we simply neglect hydrodynamic fluctuations. We carry out a standard hydrodynamic calculation, without any hadronic afterburner [37,38], and neglecting the interactions in the hadronic gas at freeze-out [39,40]. We evaluate fluctuation observables at freeze-out, in a way that matches the experimental procedure as closely as possible.

The standard observables to characterize fluctuations are cumulants of various quantities: Proton or antiproton multiplicity [6,41], net-proton number [5,24,42,43], net electric charge [1,44], net-kaon number [45,46], as well as mixtures of these (off-diagonal cumulants) [47–49]. In hydrodynamics, hadrons are emitted independently on the freeze-out surface.

Therefore, the only nontrivial information returned by the hydrodynamic calculation is, for a given event, the expected value of the number of particles in a given phase-space window. We express the cumulants in terms of these event-by-event expected values in Sec. II. We take into account the correlations arising from global conservation laws [50–52], which have proved to be crucial in describing experimental data [42]. As we shall see, the advantage of our formulation is that accurate values of cumulants can be obtained with a number of hydrodynamic events which is smaller by orders of magnitude than the number of events in an actual experiment or in a transport calculation [52,53].

In Sec. III, we implement this method using ideal hydrodynamic calculations of Au+Au collisions at $\sqrt{s_{NN}} = 200A$ GeV. We evaluate, as a function of the collision centrality, the first four cumulants of several quantities: numbers of protons and antiprotons, net-proton number (number of protons minus number of antiprotons), and net electric charge seen in a detector. We compare our results with data from the STAR Collaboration [1,24].

II. EVALUATING CUMULANTS IN EVENT-BY-EVENT HYDRODYNAMICS

A. Definitions

We first recall some useful definitions. The observable of interest is an integer, N, which is measured in every collision event. The event-to-event fluctuations of N can be characterized by its moments μ_n:

$$\mu_n \equiv \langle N^n \rangle, \tag{1}$$

where n is a positive integer, and angular brackets denote an average over an ensemble of events with the same beam energy and ions, belonging to the same centrality class. The whole series of moments can be obtained through the power series expansion of the moment generating function:

$$\langle e^{zN} \rangle = \sum_{n=0}^{\infty} \mu_n \frac{z^n}{n!}. \tag{2}$$

The cumulants C_n, with $n \geqslant 1$, are defined by the power series expansion of the logarithm [18]:

$$\ln \langle e^{zN} \rangle = \sum_{n=1}^{\infty} C_n \frac{z^n}{n!}, \tag{3}$$

Using Eqs. (2) and (3), one can express the cumulants as a function of the moments. For the first four cumulants, which we study in detail in Sec. III, the explicit expressions are

$$\begin{aligned}
C_1 &= \mu_1, \\
C_2 &= \mu_2 - \mu_1^2, \\
C_3 &= \mu_3 - 3\mu_2\mu_1 + 2\mu_1^3, \\
C_4 &= \mu_4 - 4\mu_3\mu_1 - 3\mu_2^2 + 12\mu_2\mu_1^2 - 6\mu_1^4.
\end{aligned} \tag{4}$$

The first cumulants C_1 and C_2 are the mean and the variance. The next two cumulants, C_3 and C_4, vanish if the probability distribution of N is Gaussian. They are called skewness and kurtosis.

B. Two-step averaging

We now detail the derivation of cumulants in event-by-event hydrodynamics. The most straightforward way to mimic experiment would be to take an initial condition, solve the hydrodynamic equations, emit hadrons on the freeze-out surface by Monte Carlo sampling, and repeat the whole process many times. However, solving the hydrodynamic equations is time consuming, and a faster procedure can be devised, which amounts to using the same initial conditions several times, by repeating the sampling procedure at freeze-out.

Our starting point is the observation that a hydrodynamic event is not the same thing as an experimental event, because hydrodynamics does not retain the microscopic information on particles. A single hydrodynamic simulation with given initial conditions may lead to different hadronic emissions in the end, since hadrons are emitted randomly at freeze-out. Therefore, a hydrodynamic event is actually an *ensemble* of events with the same initial conditions [54]. Then, the average over events in hydrodynamics is a two-step process. First an ensemble average over events with identical initial conditions, then an average over initial conditions:

$$\langle e^{zN} \rangle = \langle \langle e^{zN} \rangle_{\text{fo}} \rangle_{\text{ic}}, \tag{5}$$

where the subscript "fo" refers to the average over the ensemble of events at freeze-out, while the subscript "ic" refers to the average over hydrodynamic events.

C. Average at freeze-out

We now explain how the average at freeze-out is done in practice. We start with the simple case where N denotes the multiplicity of a specific particle, say, the proton multiplicity in a certain phase-space window. The only information delivered by hydrodynamics for a fixed initial condition is the expected value of N at freeze-out, which we denote by $\bar{N}$. As recalled above, the hydrodynamic description assumes that hadrons are emitted independently on the freeze-out surface. Note that this independence strictly holds only before strong decays take place. The decay chains induce correlations between the decay products. We neglect these correlations, whose effects will be studied in a forthcoming publication, and we assume that independence is still a good approximation for the stable particles which are seen experimentally.

For independent particle emission, the probability distribution of N is a Poisson distribution, which is completely specified by $\bar{N}$. This simple case is studied in Appendix. In the case of net-charge or net-baryon fluctuations, however, it is essential to take into account the global conservation law. The net charge and the net baryon number are fixed in every event for the whole collision system. Experiments see fluctuations of these numbers because they only detect a fraction of the particles.

The conservation law induces correlations between outgoing particles [50,51]. If, in a given event, there is more charge in one region of phase space, this must be compensated by less charge in the remaining phase space. These correlations are not taken into account in the standard hydrodynamic description, where the conservation laws are satisfied only on average. Sophisticated methods have been developed for

implementing conservation laws at freeze-out [55]. We choose a simplified approach, by assuming that the multiplicities of protons and antiprotons are *both* fixed for the whole collision system (in the case of net-proton fluctuations), not only their difference [51,56]. We denote by $N_{\max}$ the value of N for the whole collision system, and by α the probability for a proton to be seen in the detector [42]:

$$\alpha \equiv \frac{\bar{N}}{N_{\max}}. \tag{6}$$

The constraint $N \leqslant N_{\max}$ is then implemented by assuming that the probability of N is a binomial distribution with success probability α, rather than a Poisson distribution. The moment generating function of the binomial distribution is

$$\langle e^{zN} \rangle_{\mathrm{fo}} = (1 - \alpha + \alpha e^z)^{\bar{N}/\alpha}, \tag{7}$$

where we have used Eq. (6) to express $N_{\max}$ in terms of α and $\bar{N}$.[1] Expanding Eq. (7) to first order in z, one finds that the average value of N is $\bar{N}$, as it should. Only the higher-order moments, $\langle N^n \rangle_{\mathrm{fo}}$ with $n \geqslant 2$, depend on α. One recovers the Poisson distribution as a limiting case when $\alpha \ll 1$, as shown in the Appendix.

The generalization to the net-proton number $N_+ - N_-$, where we now denote by N_+ and N_- the numbers of protons and antiprotons, is straightforward. One assumes that, in a given hydrodynamic event, N_+ and N_- are independent variables. Applying Eq. (7) to N_+ and N_-, one obtains

$$
\begin{aligned}
\langle e^{z(N_+ - N_-)} \rangle_{\mathrm{fo}} &= \langle e^{zN_+} \rangle_{\mathrm{fo}} \langle e^{-zN_-} \rangle_{\mathrm{fo}} \\
&= (1 - \alpha_+ + \alpha_+ e^z)^{\frac{\bar{N}_+}{\alpha_+}} (1 - \alpha_- + \alpha_- e^{-z})^{\frac{\bar{N}_-}{\alpha_-}},
\end{aligned} \tag{8}
$$

where α_+ and α_- denote the average fractions of protons and antiprotons seen in the detector, which differ in general from one another.

D. Average over initial conditions

The last step is to average over initial conditions. This averaging is done for the moments, according to Eqs. (2) and (5). For the sake of illustration, we provide the explicit expressions for the first two moments of the proton distribution, which are obtained by inserting Eq. (7) into Eq. (5):

$$
\begin{aligned}
\mu_1 &= \langle \bar{N} \rangle_{\mathrm{ic}}, \\
\mu_2 &= \langle \bar{N}^2 \rangle_{\mathrm{ic}} + \langle (1 - \alpha)\bar{N} \rangle_{\mathrm{ic}}.
\end{aligned} \tag{9}
$$

Note that the fraction α of protons falling into the acceptance window of the detector depends slightly on the initial conditions of the hydrodynamic calculation, which is the reason why we keep the factor $(1 - \alpha)$ inside the average in Eq. (9).

The cumulants are then obtained from the moments using Eqs. (4). The variance is

$$
\begin{aligned}
C_2 &= \langle \bar{N}^2 \rangle_{\mathrm{ic}} + \langle (1 - \alpha)\bar{N} \rangle_{\mathrm{ic}} - \langle \bar{N} \rangle_{\mathrm{ic}}^2 \\
&= \mathrm{Var}(\bar{N}) + \langle (1 - \alpha)\bar{N} \rangle_{\mathrm{ic}}, \tag{10}
\end{aligned}
$$

---

[1]Note that Eq. (7) can be used even if $N_{\max}$ is not an integer.

where, in the last line, we have introduced the variance of $\bar{N}$ over initial conditions, $\mathrm{Var}(\bar{N}) \equiv \langle \bar{N}^2 \rangle_{\mathrm{ic}} - \langle \bar{N} \rangle_{\mathrm{ic}}^2$. The variance C_2 is the sum of two positive contributions. The first contribution corresponds to fluctuations in initial conditions. The second contribution is the average variance of the binomial distribution, which corresponds to fluctuations at freeze-out.

Similarly, the moments of the distribution of the net-proton number $N_+ - N_-$ are obtained by inserting Eq. (8) into Eq. (5). The variance is

$$C_2 = \mathrm{Var}(\bar{N}_+ - \bar{N}_-) + \langle (1 - \alpha_+)\bar{N}_+ \rangle_{\mathrm{ic}} + \langle (1 - \alpha_-)\bar{N}_- \rangle_{\mathrm{ic}}. \tag{11}$$

Note that the contributions of fluctuations at freeze-out add up for protons and antiprotons.

We do not write the explicit expressions of higher-order moments and cumulants because they are more cumbersome and bring little added value, since arbitrary orders can be obtained automatically by expanding the generating function. Note, however, that the contributions from fluctuations in initial conditions and fluctuations at freeze-out do not appear as separate terms in higher-order cumulants. They are intertwined in a nontrivial way. Therefore, initial fluctuations have a nontrivial effect on higher-order cumulants, and event-by-event hydrodynamic simulations allow us to evaluate this effect quantitatively.

III. IMPLEMENTATION AND COMPARISON WITH STAR DATA

We now illustrate the method outlined in Sec. II by carrying out an explicit calculation. We run ideal hydrodynamic simulations using the NeXSPheRIO code [57], which has been instrumental in describing event-by-event flow fluctuations at RHIC energies [58–60]. Note that the standard description of heavy-ion collisions [13] now uses viscous hydrodynamics, rather than ideal hydrodynamics. Shear viscosity [61] and baryon diffusion [62], which are included in viscous calculations, have been shown to modify the particle spectra at RHIC energies. However, the present study focuses on fluctuations, and it is widely thought that event-by-event fluctuations largely originate from the initial state at ultrarelativistic energies [63,64]. Thus one expects these observables to have limited sensitivity to transport coefficients, even though this should eventually been checked through explicit calculations.

A. Hydrodynamic setup

We simulate 10^4 Au+Au collisions at $\sqrt{s_{NN}} = 200A$ GeV, with number of participants in the range $67 \leqslant N_{\mathrm{part}} \leqslant 394$, corresponding to the 50% most central collisions [65]. We sort these events into 1% centrality classes, defined according to the number of participants. This binning is fine enough that we need not implement the "centrality bin width correction" (CBWC) method [4], which is used to correct for volume fluctuations when the analysis is done in wide centrality bins. Note that because of this fine binning, we only have 200 events per centrality bin. As will be clear from the results presented below, this is enough to obtain accurate results for cumulants up to C_4.
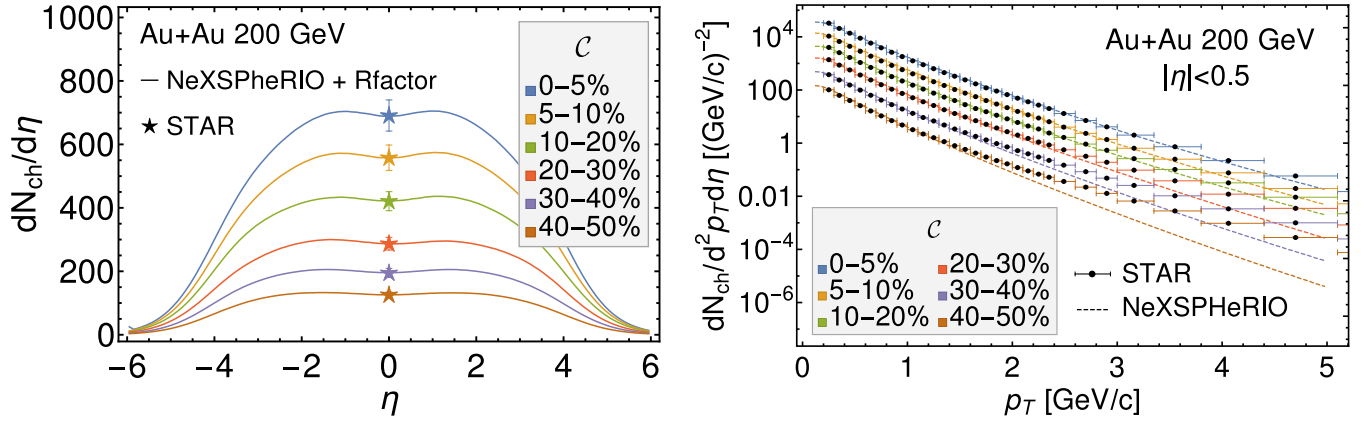
FIG. 1. Left: pseudorapidity distribution of charged hadrons in various centrality windows from our NeXSPheRIO calculation (lines) and experimental data from STAR [65]. Right: transverse momentum spectra of charged hadrons in the pseudorapidity window $|\eta| < 0.5$ from NeXSPheRIO (lines) and data from STAR [66].

In the NeXSPheRIO hydrodynamic code, the event-by-event initial conditions are borrowed from the NEXUS model [67]. We modify these initial conditions in the following way: We multiply the initial energy density with a function (Rfactor) depending on space-time rapidity, which is the same for all events in a centrality class, and which is tuned in such a way that the pseudorapidity distributions of outgoing particles has the same shape as in experiment [68]. We then run ideal hydrodynamics with this modified initial condition. Finally, the freeze-out temperature is adjusted in such a way that the transverse momentum spectrum of charged hadrons matches experimental data in the soft sector. The resulting freeze-out temperature increases mildly with the centrality percentile, from 128 to 142 MeV. The pseudorapidity and transverse momentum distributions of charged hadrons are displayed in Fig. 1. We only show experimental data from the STAR Collaboration for the sake of consistency with the following results shown in this section, where we show results on fluctuations which are also from STAR.

The emission of hadrons on the freeze-out surface is done via Monte Carlo. As explained in Sec. II C, we need to evaluate the expected value of each of the relevant multiplicities, which we have denoted by $\bar{N}$, in every hydrodynamic event. In order to reach the desired accuracy on $\bar{N}$, we repeat the Monte Carlo sampling [69] 2500 times for each hydrodynamic event.

B. Cumulants of proton, antiproton, and net-proton numbers

The STAR Collaboration has published data on the first four cumulants (C_1 to C_4) for protons, antiprotons, and the net-proton number, as a function of the collision centrality [24]. In order to evaluate these cumulants in NeXSPheRIO, as explained in Sec. II, we need to evaluate the mean numbers of protons and antiprotons $\bar{N}_+$ and $\bar{N}_-$ in each hydrodynamic event, with the same kinematic cuts as in experiment. We also need to evaluate the corresponding acceptance fractions α_+ and α_-, defined by Eq. (6). We explain how these quantities are obtained.

We cannot borrow the mean values of proton and antiproton multiplicities directly from our hydrodynamic calculation,

because the calculation is in agreement with experiment for the net-proton number but not for protons and antiprotons individually. The reason is that NeXSPheRIO was tuned to reproduce the net-proton yield near midrapidity. This is illustrated in Fig. 2. The left panel shows that our model of initial conditions underestimates baryon stopping, resulting in a proton spectrum which is too wide. In addition, the number of antiprotons is underpredicted. This is due to the fact that our freeze-out temperatures are lower than the temperature of chemical equilibration [70], at which relative abundances are reproduced. Since we do not implement partial chemical equilibrium [71,72], the number of heavy hadrons, such as antiprotons, is too small.

In order for the comparison with data to be meaningful, we rescale the calculated $\bar{N}_+$ and $\bar{N}_-$. Specifically, we multiply the calculated values of $\bar{N}_+$ and $\bar{N}_-$ by a constant which we adjust in such a way that the average values over events, denoted by C_1, coincide with the experimental values in each centrality window. Since the centrality binning is finer in our calculation than in experiment, we use linear interpolation to evaluate these multiplicative constants between two data points.

We then evaluate the fractions of protons and antiprotons, α_+ and α_-, falling into the acceptance window chosen by the STAR analysis, specifically, the rapidity window $|y| < 0.5$ and the transverse momentum window $0.4 < p_T < 0.8$ GeV/c. We proceed as follows. We first interpolate the rapidity distribution of protons and antiprotons from experiment (left of Fig. 2) using the three-source model of Ref. [73]. We then evaluate the fraction in $|y| < 0.5$, which is $\alpha_{y,+} = 0.153$ for protons, and $\alpha_{y,-} = 0.203$ for antiprotons. We assume that these fractions are independent of centrality. Next, we fit the p_T spectra (right of Fig. 2) with blast-wave fits [74]. We then evaluate the fraction in the window $0.4 < p_T < 0.8$ GeV/c, which is $\alpha_{p_T} = 0.275$ for both protons and antiprotons. Particles are detected if both y and p_T satisfy cuts, so that one must multiply the corresponding fractions $\alpha_{y,\pm}$ and α_{p_T}. We eventually obtain $\alpha_+ = 0.042$ for protons and $\alpha_- = 0.056$ for antiprotons.

Our results are presented in Fig. 3. We emphasize that the first panel, corresponding to C_1, is an input of our calculation,
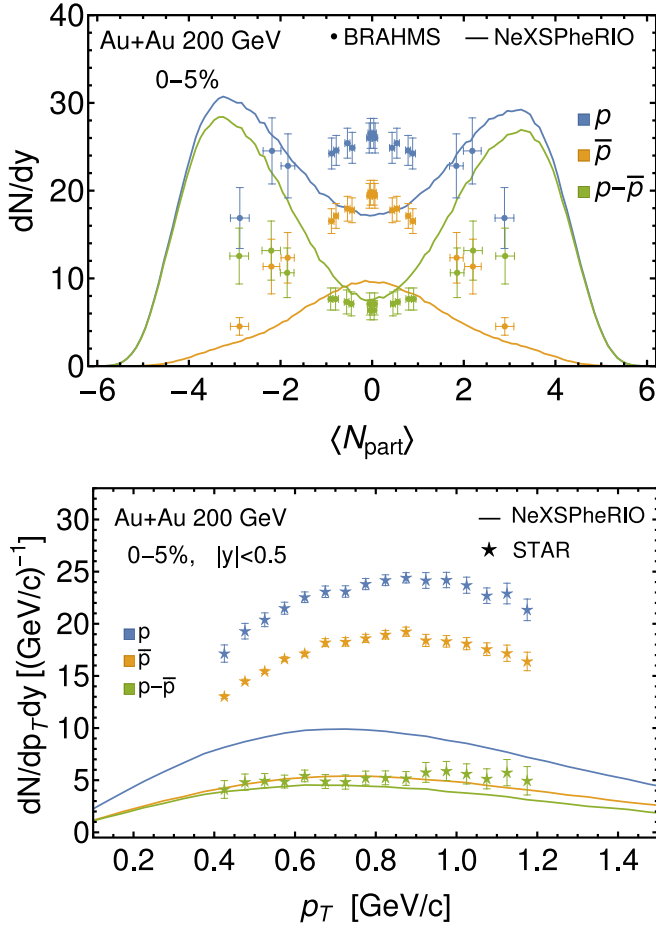
FIG. 2. Top: Rapidity distribution of protons, antiprotons, and net-proton number in the 0–5% centrality window. Lines: NeX-SPheRIO results. Symbols: experimental data from BRAHMS [68]. Bottom: Transverse momentum distribution of protons, antiprotons, and net-proton number near midrapidity (note: vertical axis is not logarithmic). Lines: NeXSPheRIO results. Symbols: data from STAR [65].

as explained above. The nontrivial output is represented by the higher-order cumulants C_2, C_3, and C_4. One first notes that the statistical error on our results, represented as a band, is very small, despite the small number of hydrodynamic events. This illustrates that our method is an efficient way of evaluating cumulants[2] in hydrodynamics.

Agreement with experiment is excellent. Higher-order cumulants are dominated by Poisson fluctuations, as detailed in the Appendix. The corrections to this baseline [56] come on the one hand from the global conservation law, and on the other hand from initial-state fluctuations. The global conservation law, quantified by the parameters α_+ and α_-, decreases

the cumulants, as illustrated by Eqs. (10) and (11) for the variance. While the correction is only ≈5% for C_2, it is larger for higher order cumulants, becoming as large as 30% for C_4.[3] Initial-state fluctuations, on the other hand, *increase* the cumulants. The effects of initial-state fluctuations and global conservation almost cancel each other out, so that the cumulants are eventually very similar to the expectation from Poisson fluctuations. This seems to be a numerical coincidence. The conclusion is that the almost perfect agreement between our calculation and experimental results is less trivial than it looks. This will be illustrated further in the Appendix.

C. Cumulants of net charge

The STAR Collaboration has also evaluated the cumulants of the net electric charge [1], defined as the difference between positive and negative charged particle multiplicities, within the pseudorapidity window $|\eta| < 0.5$ and transverse momentum window $0.2 < p_T < 2.0$ GeV/c. The evaluation of these cumulants in NeXSPheRIO is again carried out along the lines of Sec. II, where N_+ and N_- now denote the numbers of positive and negative charge particles seen in the event. We need to evaluate their mean values $\bar{N}_+$ and $\bar{N}_-$ in each hydrodynamic event, with the same kinematic cuts as in experiment, and the corresponding acceptance fractions α_+ and α_-.

As shown in Fig. 1, our code correctly reproduces the distributions of all charged particles, therefore we take the sum $\bar{N}_+ + \bar{N}_-$ directly from our calculation. However, for the same reason as our code does not reproduce the yields of identified particles, it underestimates (by ≈25%) the mean net charge at central rapidity. Therefore, we multiply the difference $\bar{N}_+ - \bar{N}_-$ from our calculation by a constant which we adjust in such a way that the average value over events, denoted by C_1, coincides with the experimental values in every centrality window.

We then evaluate the fraction α of charged particles within the kinematic cuts. We assume for simplicity that this fraction is identical for negatively and positively charged particles, that is, $\alpha_+ \simeq \alpha_-$, and we estimate it using the measured pseudorapidity distribution of charged particles [68]. The resulting value is $\alpha \approx 0.09$ and varies mildly with centrality.[4]

The width of centrality bins in our calculation is 2% for this analysis, instead of 1% in Sec. III B. This increases the number of hydrodynamic events per bin and reduces the statistical error. It is somewhat counterintuitive that one needs more statistics for an analysis which uses many more particles (all charged particles as opposed to just baryons, and in a much wider transverse momentum window). This is one of the paradoxes of cumulant analyses.

---

[2]Our calculation actually uses a value of $\alpha_\pm$ which fluctuates event to event, and is evaluated in the following way. We evaluate $\alpha_\pm$ using Eq. (6) for each hydrodynamic event. We then rescale it in such a way that the average over events matches the value calculated from measured spectra. We have checked that our results are essentially insensitive to these event-to-event fluctuations of $\alpha_\pm$.

---

[3]Specifically, the cumulants of the binomial distribution, which are obtained by inserting Eq. (7) into Eq. (3), are smaller than those of the Poisson distribution by a factor $(1 - \alpha)$ for C_2, $(1 - \alpha)(1 - 2\alpha)$ for C_3, and $(1 - \alpha)(1 - 6\alpha + 6\alpha^2)$ for C_4.

[4]As the collision becomes more central, α increases slightly due to increased stopping. We obtain $\alpha = 0.0975, 0.0944, 0.0924, 0.0901, 0.0884, 0.0858$ in the 0–5%, 5–10%, 10–20%, 20–30%, 30–40%, 40–50% centrality windows.
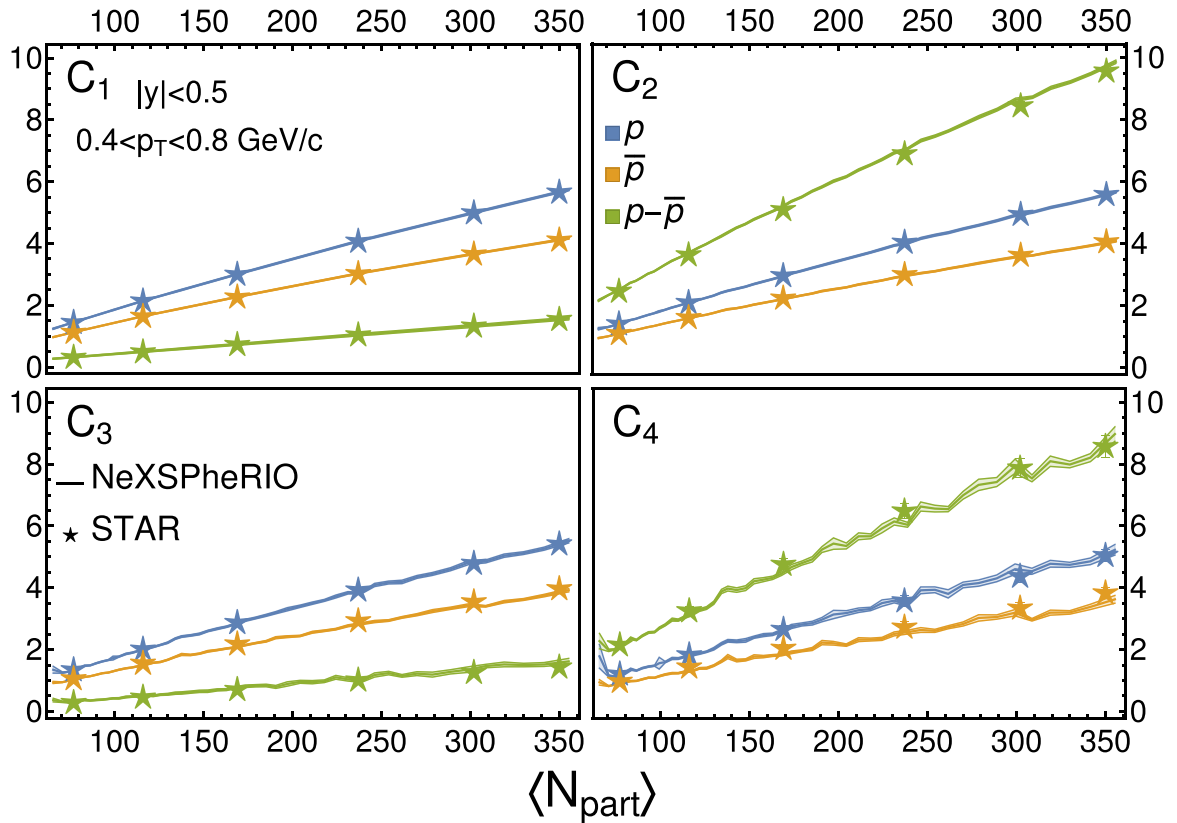
FIG. 3. Cumulants (C_1 to C_4) of p, $\bar{p}$, and $p - \bar{p}$ in Au+Au collisions at $\sqrt{s_{NN}} = 200$ GeV from our calculation (solid lines) and experiment (symbols) [24], as a function of the number of participants, which measures the collision centrality. Note that the calculation has been rescaled so as to match experiment for C_1 (see text for details). Error bands in simulation are evaluated by jackknife resampling.

Our results are presented in Fig. 4, together with experimental data from the STAR Collaboration [1]. As in Fig. 3, the first cumulant C_1 is an input of our calculation, and the nontrivial output is represented by the higher-order cumulants. The presentation differs from Fig. 3, where we had plotted the cumulants C_n themselves, in order to illustrate that they are dominated by Poisson fluctuations. In Fig. 4, we plot $\sigma \equiv \sqrt{C_2}$ instead of C_2. Physically, σ represents the standard deviation of the net charge event to event. It is interesting to note that it is larger than the mean C_1, which illustrates the small charge asymmetry at this energy. Our calculation overestimates the value of σ, and we have not yet been able to spot the origin of this discrepancy.

The higher order cumulants C_3 and C_4 are normalized by appropriate powers of σ. The resulting values of skewness and kurtosis, referred to as "standardized," measure the relative deviation to a Gaussian distribution. Figure 3 shows that calculated values are in good agreement with experiment. The small values of the skewness and kurtosis, at the percent level, illustrate that net-charge fluctuations are almost Gaussian. The standardized kurtosis decreases as a function of N_{part}. This is an illustration of the central limit theorem, from which one expects that fluctuations come closer to a Gaussian as the system size increases. If one neglects the effect of the global charge conservation, that is, if one sets the parameter α to zero, the kurtosis C_4 is larger by a factor ≈ 2, and agreement with data is lost. This illustrates that

the agreement of our calculation with data is a nontrivial achievement.

IV. DISCUSSION

We have introduced an efficient method for evaluating cumulants of conserved charges in event-by-event hydrodynamic simulations of heavy-ion collisions. As far as we know, this is the first time that cumulants have been computed with event-by-event hydrodynamics incorporating both fluctuations in the initial conditions and in the freeze-out. Our approach is based on a simplified treatment of fluctuations at freeze-out. Specifically, we assume that the multiplicity of a given identified particle, in a given phase-space window, follows a binomial distribution. We further assume that the "success probability," which is one of the two parameters of the binomial, coincides with the acceptance fraction covered by the detector. This amounts to assuming that the total multiplicity of a given particle is the same in all events, which is a practical way of implementing global number (baryonic or charge) conservation. Even though we have chosen to apply our method to the top RHIC energy, this particular assumption is actually better justified at lower energies, where particle creation is scarce, and the protons after the collision are those in the colliding nuclei, whose number does not fluctuate. Therefore, our approach should still be valid in the vicinity of a critical point. Critical fluctuations should result in increased
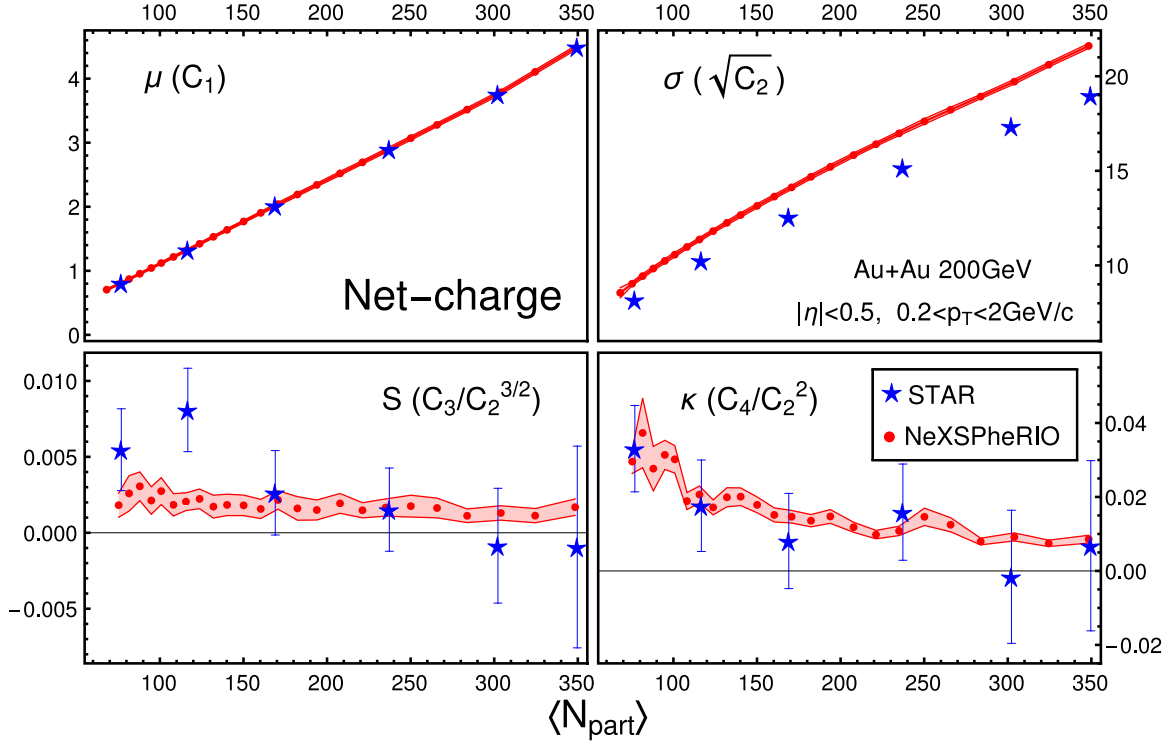
FIG. 4. Centrality dependence of cumulants of the net charge in Au+Au collisions at $\sqrt{s_{NN}} = 200$ GeV, from our hydrodynamic calculation (solid lines) and experiment (symbols) [1]. As in Fig. 3, the calculated C_1 has been rescaled to match data (see text for details).

event-to-event fluctuations in the hydrodynamic phase, thus amplifying the effect of fluctuations in the initial conditions, but should not affect the freeze-out itself. Note, however, that assuming a binomial distribution at freeze-out amounts to assuming that particles are uncorrelated except for a global conservation law. In this respect, we neglect correlations that might arise from final-state interactions or resonance decays.

We have illustrated the power of this method with ideal hydrodynamic simulations of Au+Au collisions at 200 GeV. Accurate results have been obtained for the first four cumulants of various quantities (proton and antiproton multiplicities, net-proton number, net electric charge) with only a few hundred hydrodynamic events per centrality bin. This is smaller by orders of magnitude than the number of events in actual experiments, or in transport calculations [52,53,75]. The reason behind this spectacular improvement is that a hydrodynamic event is not equivalent to a single event in an experiment or a transport calculation. It represents an ensemble of events in the thermodynamic sense, which contains much more information. We carry out a separation between initial-state fluctuations and freeze-out which fully exploits this property. Since the nontrivial higher-order cumulants observed in data mostly originate from event-to-event fluctuations in the initial state (which can be understood as volume fluctuations), they can be captured with a modest number of initializations. Generalization of our method to other quantities, such as the net-kaon number or off-diagonal cumulants [48], and to higher-order cumulants [43] is straightforward.

Due to discrepancies between our calculation and experiment, concerning the spectra of identified particles, we had to rescale the average number of particles in the acceptance

window, corresponding to the first cumulant C_1, so as to match data. With this rescaling, calculated values of higher-order cumulants (C_2 to C_4) are in excellent agreement with experiment for net-proton fluctuations, and in fair agreement for net-charge fluctuations. This is a nontrivial achievement, which results from taking into account both the global conservation law, and event-to-event fluctuations. We are working on improving our description in such a way that no rescaling is needed. Specifically, we are developing an improved description based on smearing partons from the AMPT transport model, inspired on what was done in [76,77]. The aim is to correctly describe both the (pseudo)rapidity distributions and transverse momentum spectra for a range of energies for charged particles, protons and antiprotons.

One should keep in mind that the measured cumulants are dominated by Poisson fluctuations, which are essentially trivial. Poisson fluctuations can be removed by replacing moments with factorial moments [78]. This is achieved by replacing e^z with $1 + z$ in the left-hand side of Eq. (2). μ_n in the right-hand side of Eqs. (2) then becomes the factorial moment, which is the average number of n-tuples per event. Factorial cumulants are related to factorial moments in the same way as cumulants are related to moments, i.e., through Eq. (4). The factorial cumulant of order n measures the n-particle correlation [79,80], and can be used for probing critical fluctuations [81]. Factorial cumulants can be evaluated in event-by-event hydrodynamics along the same lines as cumulants. One need simply replace e^z with $1 + z$ in Eqs. (5) and (7). Note, finally, that the definition of factorial cumulants can be amended to remove not only Poisson fluctuations, but also the trivial correlation from the global conservation law [82],
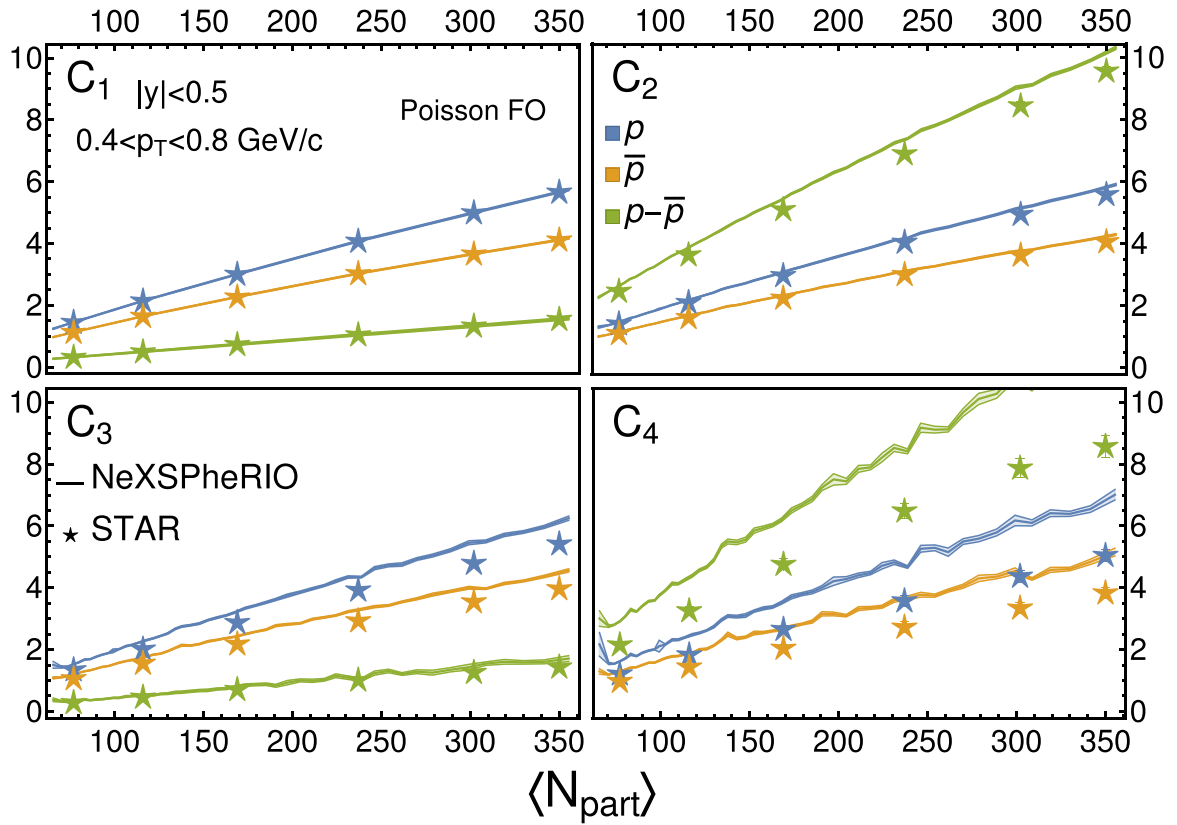
FIG. 5. Similar to Fig. 3, where the lines now denote the results of our calculations assuming independent particle emission at freeze-out, i.e., neglecting the correlations from the global conservation law.

so as to isolate nontrivial correlations and effects of initial state fluctuations. We intend to use these modified cumulants in conjunction with an equation of state with an adjustable critical point position [83,84].

APPENDIX: POISSON DISTRIBUTION

In this Appendix, we study the simple case where particles are emitted independently at freeze-out, neglecting the correlation from the global conservation law. Independent particle emission implies that the distribution of any multiplicity N at freeze-out is a Poisson distribution. The moment generating function is

$$\langle e^{zN} \rangle_{\text{fo}} = \exp((e^z - 1)\bar{N}), \qquad (A1)$$

where $\bar{N}$ is the mean value of N. An elementary calculation shows that Eq. (7) reduces to Eq. (A1) for $\alpha \ll 1$. This shows

that the binomial distribution reduces to a Poisson distribution in this limit.

If there are no fluctuations in initial conditions, then, inserting Eq. (A1) into Eq. (3), one obtains immediately the cumulants of the distribution of N:

$$C_n = \bar{N}. \qquad (A2)$$

The cumulants of the Poisson distribution are all equal. This is approximately true for the measured cumulants of the numbers of protons and antiprotons in Fig. 3 (circles and squares), where one readily notices that $C_1 \approx C_2 \approx C_3 \approx C_4$ for all centralities. This suggests that Poisson fluctuations are the dominant source of fluctuations.

If the multiplicities of protons and antiprotons, N_+ and N_-, are independent and both follow a Poisson distribution, then the moment generating function of the net-proton number $N_+ - N_-$ is

$$\langle e^{z(N_+ - N_-)} \rangle_{\text{fo}} = \exp[(e^z - 1)\bar{N}_+ + (e^{-z} - 1)\bar{N}_-]. \qquad (A3)$$

If there are no fluctuations in initial conditions, then, inserting Eq. (A3) into Eq. (3), one obtains the cumulants of the distribution of $N_+ - N_-$ (known as the Skellam distribution):

$$C_{2n-1} = \bar{N}_+ - \bar{N}_-,$$
$$C_{2n} = \bar{N}_+ + \bar{N}_-. \qquad (A4)$$

Looking at the measured cumulants of the net-proton number in Fig. 3 (stars), one notices that $C_1 \approx C_3$ and

$C_2 \approx C_4$, which again suggests that Skellam fluctuations dominate.

In event-by-event hydrodynamics, however, initial-state fluctuations have a sizable effect, and break the simple equalities (A2) and (A4). This is illustrated by Fig. 5, in which the lines display the results of our event-by-event hydrodynamic calculation, assuming independent particle emission at freeze-out. Fluctuations in initial conditions increase higher-order cumulants, in particular C_4, so that our calculation overshoots the data. Agreement with data is only restored after taking into account the correlations from the global conservation law, as shown in Fig. 3.

---

[1] L. Adamczyk *et al.* (STAR Collaboration), Phys. Rev. Lett. **113**, 092301 (2014).

[2] M. A. Stephanov, K. Rajagopal, and E. V. Shuryak, Phys. Rev. Lett. **81**, 4816 (1998).

[3] K. Fukushima and T. Hatsuda, Rep. Prog. Phys. **74**, 014001 (2011).

[4] X. Luo and N. Xu, Nucl. Sci. Technol. **28**, 112 (2017).

[5] J. Adam *et al.* (STAR Collaboration), Phys. Rev. Lett. **126**, 092301 (2021).

[6] M. Abdallah *et al.* (STAR Collaboration), Phys. Rev. C **104**, 024902 (2021).

[7] S. Borsanyi, Z. Fodor, S. D. Katz, S. Krieg, C. Ratti, and K. Szabo, J. High Energy Phys. 01 (2012) 138.

[8] S. Borsanyi, Z. Fodor, J. N. Guenther, S. K. Katz, K. K. Szabo, A. Pasztor, I. Portillo, and C. Ratti, J. High Energy Phys. 10 (2018) 205.

[9] A. Bazavov, H. T. Ding, P. Hegde, O. Kaczmarek, F. Karsch, E. Laermann, S. Mukherjee, P. Petreczky, C. Schmidt, D. Smith *et al.*, Phys. Rev. Lett. **109**, 192302 (2012).

[10] S. Borsanyi, Z. Fodor, S. D. Katz, S. Krieg, C. Ratti, and K. K. Szabo, Phys. Rev. Lett. **111**, 062005 (2013).

[11] P. Alba, W. Alberico, R. Bellwied, M. Bluhm, V. Mantovani Sarti, M. Nahrgang, and C. Ratti, Phys. Lett. B **738**, 305 (2014).

[12] A. Bazavov, D. Bollweg, H. T. Ding, P. Enns, J. Goswami, P. Hegde, O. Kaczmarek, F. Karsch, R. Larsen, S. Mukherjee *et al.*, Phys. Rev. D **101**, 074502 (2020).

[13] C. Gale, S. Jeon, and B. Schenke, Int. J. Mod. Phys. A **28**, 1340011 (2013).

[14] P. Romatschke and U. Romatschke, *Relativistic Fluid Dynamics In and Out of Equilibrium And Applications to Relativistic Nuclear Collisions*, Cambridge Monographs on Mathematical Physics (Cambridge University Press, Cambridge, 2019).

[15] J. E. Bernhard, J. S. Moreland, and S. A. Bass, Nat. Phys. **15**, 1113 (2019).

[16] G. Nijs, W. van der Schee, U. Gürsoy, and R. Snellings, Phys. Rev. C **103**, 054909 (2021).

[17] D. Everett *et al.* (JETSCAPE Collaboration), Phys. Rev. C **103**, 054904 (2021).

[18] M. Asakawa and M. Kitazawa, Prog. Part. Nucl. Phys. **90**, 299 (2016).

[19] M. A. Stephanov, K. Rajagopal, and E. V. Shuryak, Phys. Rev. D **60**, 114028 (1999).

[20] S. Borsanyi, Z. Fodor, S. D. Katz, S. Krieg, C. Ratti, and K. K. Szabo, Phys. Rev. Lett. **113**, 052301 (2014).

[21] M. Bluhm, A. Kalweit, M. Nahrgang, M. Arslandok, P. Braun-Munzinger, S. Floerchinger, E. S. Fraga, M. Gazdzicki, C. Hartnack, C. Herold *et al.*, Nucl. Phys. A **1003**, 122016 (2020).

[22] O. Socolowski, Jr., F. Grassi, Y. Hama, and T. Kodama, Phys. Rev. Lett. **93**, 182301 (2004).

[23] C. Shen and B. Schenke, Phys. Rev. C **97**, 024907 (2018).

[24] L. Adamczyk *et al.* (STAR Collaboration), Phys. Rev. Lett. **112**, 032302 (2014).

[25] E. Calzetta, Class. Quantum Grav. **15**, 653 (1998).

[26] J. I. Kapusta, B. Muller, and M. Stephanov, Phys. Rev. C **85**, 054906 (2012).

[27] X. An, G. Basar, M. Stephanov, and H. U. Yee, Phys. Rev. C **100**, 024910 (2019).

[28] N. Mirón-Granese, A. Kandus, and E. Calzetta, J. High Energy Phys. 07 (2020) 064.

[29] M. Pradeep, K. Rajagopal, M. Stephanov, and Y. Yin, Phys. Rev. D **106**, 036017 (2022).

[30] L. Jiang, P. Li, and H. Song, Phys. Rev. C **94**, 024918 (2016).

[31] M. Nahrgang, M. Bluhm, T. Schäfer, and S. A. Bass, Phys. Rev. D **99**, 116015 (2019).

[32] M. Pradeep, K. Rajagopal, M. Stephanov, and Y. Yin, PoS **(CPOD2021)**, 035 (2022).

[33] L. Yan and H. Grönqvist, J. High Energy Phys. 03 (2016) 121.

[34] Y. Akamatsu, A. Mazeliauskas, and D. Teaney, Phys. Rev. C **95**, 014909 (2017).

[35] A. Sakai, K. Murase, and T. Hirano, Phys. Rev. C **102**, 064903 (2020).

[36] X. An, G. Başar, M. Stephanov, and H. U. Yee, Phys. Rev. Lett. **127**, 072301 (2021).

[37] H. Petersen, J. Steinheimer, G. Burau, M. Bleicher, and H. Stöcker, Phys. Rev. C **78**, 044901 (2008).

[38] H. Song, S. A. Bass, U. Heinz, T. Hirano, and C. Shen, Phys. Rev. Lett. **106**, 192301 (2011); **109**, 139904(E) (2012).

[39] V. Vovchenko and V. Koch, Phys. Rev. C **103**, 044903 (2021).

[40] V. Vovchenko, V. Koch, and C. Shen, Phys. Rev. C **105**, 014904 (2022).

[41] J. Adamczewski-Musch *et al.* (HADES Collaboration), Phys. Rev. C **102**, 024914 (2020).

[42] S. Acharya *et al.* (ALICE Collaboration), Phys. Lett. B **807**, 135564 (2020).

[43] M. Abdallah *et al.* (STAR Collaboration), Phys. Rev. Lett. **127**, 262301 (2021).

[44] A. Adare *et al.* (PHENIX Collaboration), Phys. Rev. C **93**, 011901 (2016).

[45] L. Adamczyk *et al.* (STAR Collaboration), Phys. Lett. B **785**, 551 (2018).

[46] R. Bellwied, J. Noronha-Hostler, P. Parotto, I. Portillo Vazquez, C. Ratti, and J. M. Stafford, Phys. Rev. C **99**, 034912 (2019).

[47] H. T. Ding, S. Mukherjee, H. Ohno, P. Petreczky, and H. P. Schadler, Phys. Rev. D **92**, 074043 (2015).

[48] J. Adam *et al.* (STAR Collaboration), Phys. Rev. C **100**, 014902 (2019); **105**, 029901(E) (2022).

[49] R. Bellwied, S. Borsanyi, Z. Fodor, J. N. Guenther, J. Noronha-Hostler, P. Parotto, A. Pasztor, C. Ratti, and J. M. Stafford, Phys. Rev. D **101**, 034506 (2020).

[50] N. Borghini, P. M. Dinh, and J. Y. Ollitrault, Phys. Rev. C **62**, 034902 (2000).

[51] A. Bzdak, V. Koch, and V. Skokov, Phys. Rev. C **87**, 014901 (2013).

[52] J. Hammelmann and H. Elfner, arXiv:2202.11417.

[53] J. Xu, S. Yu, F. Liu, and X. Luo, Phys. Rev. C **94**, 024901 (2016).

[54] R. Derradi de Souza, T. Koide, and T. Kodama, Prog. Part. Nucl. Phys. **86**, 35 (2016).

[55] D. Oliinychenko and V. Koch, Phys. Rev. Lett. **123**, 182302 (2019).

[56] X. Luo, B. Mohanty, and N. Xu, Nucl. Phys. A **931**, 808 (2014).

[57] C. E. Aguiar, Y. Hama, T. Kodama, and T. Osada, Nucl. Phys. A **698**, 639 (2002).

[58] R. Andrade, F. Grassi, Y. Hama, T. Kodama, and O. Socolowski Jr., Phys. Rev. Lett. **97**, 202302 (2006).

[59] J. Takahashi, B. M. Tavares, W. L. Qian, R. Andrade, F. Grassi, Y. Hama, T. Kodama, and N. Xu, Phys. Rev. Lett. **103**, 242301 (2009).

[60] F. G. Gardim, F. Grassi, M. Luzum, and J. Y. Ollitrault, Phys. Rev. Lett. **109**, 202302 (2012).

[61] I. A. Karpenko, P. Huovinen, H. Petersen, and M. Bleicher, Phys. Rev. C **91**, 064901 (2015).

[62] G. S. Denicol, C. Gale, S. Jeon, A. Monnai, B. Schenke, and C. Shen, Phys. Rev. C **98**, 034916 (2018).

[63] B. Alver and G. Roland, Phys. Rev. C **81**, 054905 (2010); **82**, 039903(E) (2010).

[64] M. Luzum and H. Petersen, J. Phys. G: Nucl. Part. Phys. **41**, 063102 (2014).

[65] B. I. Abelev *et al.* (STAR Collaboration), Phys. Rev. C **79**, 034909 (2009).

[66] J. Adams *et al.* (STAR Collaboration), Phys. Rev. Lett. **91**, 172302 (2003).

[67] H. J. Drescher, F. M. Liu, S. Ostapchenko, T. Pierog, and K. Werner, Phys. Rev. C **65**, 054902 (2002).

[68] I. G. Bearden *et al.* (BRAHMS Collaboration), Phys. Rev. Lett. **88**, 202301 (2002).

[69] F. G. Gardim, F. Grassi, Y. Hama, M. Luzum, and J. Y. Ollitrault, Phys. Rev. C **83**, 064901 (2011).

[70] A. Andronic, P. Braun-Munzinger, K. Redlich, and J. Stachel, Nature (London) **561**, 321 (2018).

[71] P. Huovinen, Eur. Phys. J. A **37**, 121 (2008).

[72] P. Huovinen and P. Petreczky, Nucl. Phys. A **837**, 26 (2010).

[73] L. N. Gao, F. H. Liu, Y. Sun, Z. Sun, and R. A. Lacey, Eur. Phys. J. A **53**, 61 (2017).

[74] E. Schnedermann, J. Sollfrank, and U. W. Heinz, Phys. Rev. C **48**, 2462 (1993).

[75] S. He and X. Luo, Phys. Lett. B **774**, 623 (2017).

[76] C. Chattopadhyay, R. S. Bhalerao, J. Y. Ollitrault, and S. Pal, Phys. Rev. C **97**, 034915 (2018).

[77] B. Fu, K. Xu, X. G. Huang, and H. Song, Phys. Rev. C **103**, 024903 (2021).

[78] M. Kitazawa and X. Luo, Phys. Rev. C **96**, 024910 (2017).

[79] A. Bzdak, V. Koch, and N. Strodthoff, Phys. Rev. C **95**, 054906 (2017).

[80] P. Di Francesco, M. Guilbaud, M. Luzum, and J. Y. Ollitrault, Phys. Rev. C **95**, 044911 (2017).

[81] B. Ling and M. A. Stephanov, Phys. Rev. C **93**, 034915 (2016).

[82] R. Rogly, G. Giacalone, and J. Y. Ollitrault, Phys. Rev. C **99**, 034902 (2019).

[83] P. Parotto, M. Bluhm, D. Mroczek, M. Nahrgang, J. Noronha-Hostler, K. Rajagopal, C. Ratti, T. Schäfer, and M. Stephanov, Phys. Rev. C **101**, 034901 (2020).

[84] J. M. Karthein, D. Mroczek, A. R. Nava Acuna, J. Noronha-Hostler, P. Parotto, D. R. P. Price, and C. Ratti, Eur. Phys. J. Plus **136**, 621 (2021).